Comparison of electrostatic and electromagnetic simulations for very high frequency plasmas

Yu-Ru Zhang,[1] Xiang Xu,[1] Shu-Xia Zhao,[1,2] A. Bogaerts,[2] and You-Nian Wang[1,a)]
[1]*School of Physics and Optoelectronic Technology, Dalian University of Technology, Dalian 116024, China*
[2]*Department of Chemistry, University of Antwerp, Campus Drie Eiken, Universiteitsplein 1, BE-2610 Wilrijk-Antwerp, Belgium*

(Received 25 October 2010; accepted 1 November 2010; published online 22 November 2010)

A two-dimensional self-consistent fluid model combined with the full set of Maxwell equations is developed to investigate an argon capacitively coupled plasma, focusing on the electromagnetic effects on the discharge characteristics at various discharge conditions. The results indicate that there exist distinct differences in plasma characteristics calculated with the so-called electrostatic model (i.e., without taking into account the electromagnetic effects) and the electromagnetic model (which includes the electromagnetic effects), especially at very high frequencies. Indeed, when the excitation source is in the high frequency regime and the electromagnetic effects are taken into account, the plasma density increases significantly and meanwhile the ionization rate evolves to a very different distribution when the electromagnetic effects are dominant. Furthermore, the dependence of the plasma characteristics on the voltage and pressure is also investigated, at constant frequency. It is observed that when the voltage is low, the difference between these two models becomes more obvious than at higher voltages. As the pressure increases, the plasma density profiles obtained from the electromagnetic model smoothly shift from edge-peaked over uniform to a broad maximum in the center. In addition, the edge effect becomes less pronounced with increasing frequency and pressure, and the skin effect rather than the standing-wave effect becomes dominant when the voltage is high. © *2010 American Institute of Physics*. [doi:10.1063/1.3519515]

I. INTRODUCTION

Capacitively coupled plasmas (CCPs) are widely used to fabricate very large scale integrated circuits,[1] most notably in deposition of thin films and etching of semiconductor and metal surfaces. It is well known that a higher frequency produces higher-density plasmas with lower-energy ions.[2,3] Thus the very high frequency (VHF) plasma source has attracted growing interest and is now widely used in the silicon wafer and flat panel display processing, due to the good quality films at high deposition rates.[4,5] However, when the excitation wavelength becomes comparable to the electrode dimension at high frequencies, the electromagnetic effects, such as standing-wave effect and skin effect,[6] start to have a profound influence on the plasma properties. It is important to understand this influence, in order to control the discharge parameters and optimize the plasma technique.

In recent years, several theoretical studies[6–21] and experimental research[22–30] have been published on the plasma characteristics in a CCP sustained by VHF sources. Lieberman *et al.*[6] first employed a uniform slab model to investigate the standing-wave and skin effects in VHF discharges. The work of Sansonnens and Schmitt[7] showed that the radial inhomogeneity caused by the standing-wave effect could be removed by replacing one of the electrodes with a shaped one. Subsequently, Sansonnens[8] presented a two-dimensional quasiplanar circuit model to explain that the shape of the plasma characteristics was determined by many factors in large rectangular reactors. Chabert *et al.*[9,10] used a transmission line model derived from the electromagnetic field, and came to the conclusion that the discharge experienced a transition from E mode (i.e., sustained by a capacitive field) to H mode (i.e., sustained by an inductive field), as the voltage increased. Lee *et al.*[11] focused on the coupling of the electromagnetic effects with the electrostatic edge effect in a two-dimensional axisymmetric model, and they observed the so-called stop band at higher frequencies and higher pressures. Rauf *et al.*[12,13] developed a fluid model to simulate an argon plasma, discovering that the plasma density peaked at the chamber center under the condition where the electromagnetic effects were predominant. Furthermore, they also observed that the plasma became more uniform for a small interelectrode gap at 180 MHz. More recently, Chen *et al.*[14] presented a three-dimensional model to examine the behavior of H_2 plasmas in a large-area rectangular reactor from 13.56 to 200 MHz. Besides, considerable effort has also been made on studying the discharge mechanisms with dual frequency excitation in the VHF regime.[15–21] Yang and Kushner[19–21] utilized a full-wave Maxwell solver, and studied the properties of plasmas sustained in Ar and Ar/CF_4 at different discharge conditions.

In addition, some experiments have been put forward to investigate the electromagnetic effects. Satake *et al.*[22] measured the voltage distribution with VHF excitation by a high frequency voltage probe, and it agreed well with the plasma distribution. Schmidt *et al.*[23] measured the optical emission intensity and ion flux in a cylindrical reactor, proving that the Gaussian-lens electrode could suppress the standing wave nonuniformity. Subsequently they performed measurements

a)Electronic mail: ynwang@dlut.edu.cn.

in large area rectangular reactors, showing that a thin conducting layer present on the dielectric plate was sufficient to screen the electrode shape effect.[24] Miller *et al.*[25,26] reported the magnetic field and other plasma parameters, for instance, line-integrated electron density and ion saturation current, as a function of frequency. Recently, Ahn and Chang[27] revealed, by means of a Langmuir probe and a B-dot probe, that the strong plasma inhomogeneity, detected in a cylindrical high frequency capacitive discharge at high pressures, was created by the significant inductive electric field near the radial edge. Moreover, Sung *et al.*[28–30] verified experimentally that the plasma nonuniformity could be suppressed by controlling the phase shift between the VHF voltages.

However, there still remain some questions with regard to electromagnetic effects in the CCP discharge excited by VHF sources. For instance, in most of the models mentioned above, the emphasis is mainly put on the plasma characteristics at various discharge conditions when the electromagnetic effects are considered. However, the differences between the so-called electrostatic model (with only the static electric field taken into account), and the electromagnetic model (with the electromagnetic effects taken into account) are still not completely clear, especially when the electromagnetic effects contribute significantly to the discharge process, as in the case of very high frequencies. The purpose of this article is to establish a two-dimensional fluid model, including the full set of Maxwell equations, to systematically examine the differences between the so-called electrostatic model and the electromagnetic model for different discharge conditions, in order to obtain more insight in the electromagnetic effects.

This paper is outlined as follows. In Sec. II, the fluid model for the CCP which includes the full set of Maxwell equations, as well as the boundary conditions used in the model, is presented. The differences between the plasma characteristics as obtained from the so-called electrostatic model and the electromagnetic model at various frequencies, voltages, and pressures in a CCP are shown in Sec. III. Finally, a summary is given in Sec. IV.

II. DESCRIPTION OF THE FLUID MODEL

In this section, the equations for the fluid model, including the full set of Maxwell equations, together with the boundary conditions are presented. In our model, the gap between the two electrodes is L. The upper electrode with radius R $(z=L)$ and the cylindrical wall $(r=R)$ are grounded; the lower electrode with radius R_{powered} $(z=0)$ is driven by the radio frequency (rf) source, $V=V_0 \sin(wt)$, where w and V_0 are the frequency and the peak voltage of the rf source, respectively. A schematic picture of the CCP reactor is shown in Fig. 1.

The plasma, which can be treated as a continuum, consists of electrons and Ar^+ ions, whose behavior can be described by continuity equations, momentum balance equations, and an energy balance equation for the electrons. No energy balance equation is needed for ions because they can be assumed to be at room temperature. Since the electron mass is very small, we can ignore the inertial term, so the electron flux can be presented in the drift-diffusion form.

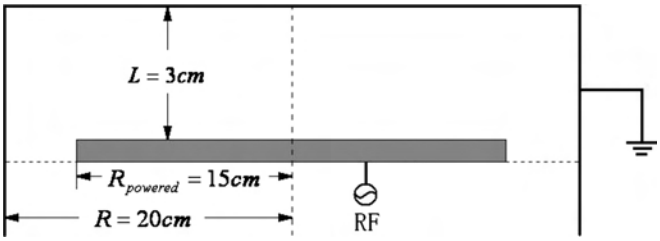

FIG. 1. Schematic picture of the cylindrical CCP reactor configuration.

In the electromagnetic model, the equations for the electrons are as follows

$$\frac{\partial n_e}{\partial t} + \nabla \cdot \mathbf{j_e} = k_i N n_e, \tag{1}$$

$$\mathbf{j_e} = -\frac{1}{m_e \nu_{en}} \nabla (n_e k_B T_e) - \frac{e n_e}{m_e \nu_{en}} (\mathbf{E} + \mathbf{u_e} \times \mathbf{B}), \tag{2}$$

$$\frac{\partial \frac{3}{2} n_e k_B T_e}{\partial t} = -\nabla \cdot \mathbf{q_e} - e\mathbf{E} \cdot \mathbf{j_e} - H_i k_i N n_e, \tag{3}$$

where the flux of energy $\mathbf{q_e}$ is given by

$$\mathbf{q_e} = \frac{5}{2} k_B T_e \mathbf{j_e} - \frac{5}{2} \frac{n_e k_B T_e}{m_e \nu_{en}} \nabla (k_B T_e). \tag{4}$$

Here n_e is the electron density and N is the neutral gas density; $\mathbf{j_e}$, $\mathbf{u_e}$, m_e, and T_e are the flux, velocity, mass, and temperature of the electrons, respectively; $\mathbf{E}$ is the electric field, consisting of a static electric field and a vortex electric field, and $\mathbf{B}$ is the magnetic field; H_i is the ionization energy, and the ionization coefficient k_i, and the electron-neutral collision frequency ν_{en} are adopted from Ref. 31.

For the Ar^+ ions, we adopt the momentum balance equations based on the cold fluid approximation

$$\frac{\partial n_i}{\partial t} + \nabla \cdot (n_i \mathbf{u_i}) = k_i N n_e, \tag{5}$$

$$\frac{\partial (n_i m_i \mathbf{u_i})}{\partial t} + \nabla \cdot (n_i m_i \mathbf{u_i} \mathbf{u_i}) = e n_i \mathbf{E} - \frac{1}{2} m_i n_i \nu_{in} \mathbf{u_i}. \tag{6}$$

Here n_i, $\mathbf{u_i}$, and m_i are the ion density, ion velocity, and ion mass, respectively; the ion temperature T_i is assumed being constant as room temperature, as mentioned above, and ν_{in} is the ion-neutral collision frequency obtained from Ref. 32.

The self-consistently calculated electric field and magnetic field are obtained from the full set of Maxwell equations

$$\nabla \times \mathbf{E} = -\frac{\partial \mathbf{B}}{\partial t}, \tag{7}$$

$$\nabla \times \mathbf{B} = \mu_0 \mathbf{J} + \mu_0 \varepsilon_0 \frac{\partial \mathbf{E}}{\partial t}, \tag{8}$$

$$\nabla \cdot \mathbf{E} = \frac{e}{\varepsilon_0}(n_i - n_e), \tag{9}$$

$$\nabla \cdot \mathbf{B} = 0, \tag{10}$$

where μ_0 and ε_0 are the vacuum permeability and the permittivity, respectively; the current density is expressed as $\mathbf{J} = e(n_i \mathbf{u_i} - \mathbf{j_e})$.

Introducing the electric potential ϕ and the magnetic vector potential $\mathbf{A}$, the electric field can be given as $\mathbf{E} = -\nabla\phi + \mathbf{E_T}$, where $\mathbf{E_T} = -\partial\mathbf{A}/\partial t$ is the vortex electric field. Furthermore, we can arrange that $\nabla \cdot \mathbf{E_T} = 0$ by making use of the Coulomb gauge $\nabla \cdot \mathbf{A} = 0$. This reduces the full set of Maxwell equations to

$$\nabla^2 \phi = \frac{e}{\varepsilon_0}(n_e - n_i), \tag{11}$$

$$\nabla^2 \mathbf{E_T} - \mu_0 \varepsilon_0 \frac{\partial^2 \mathbf{E_T}}{\partial t^2} = \mu_0 \frac{\partial \mathbf{J}}{\partial t} - \mu_0 \varepsilon_0 \frac{\partial^2 \nabla \phi}{\partial t^2}. \tag{12}$$

The boundary conditions of $\mathbf{j_e}$ and $\mathbf{q_e}$ used in the fluid simulation at all walls, i.e., $z=0$, $z=L$, and $r=R$ are as follows

$$\mathbf{j_e} = \mp \frac{1-\Theta}{4} n_e \sqrt{\frac{8 k_B T_e}{m_e \pi}}, \tag{13}$$

$$\mathbf{q_e} = \frac{5}{2} \mathbf{j_e} k_B T_e, \tag{14}$$

where Θ is the electron reflection coefficient. Meanwhile, we assume that the ion density and the ion velocity do not change substantially near the wall, so the gradients are set to zero at the walls, i.e., $\nabla n_i = 0$, and $\nabla \cdot \mathbf{u_i} = 0$. All external materials are assumed to be perfect electric conductors, so the boundary conditions of $\mathbf{E_T}$ are $\partial \mathbf{E_{Tz}}/\partial z = 0$ and $\partial(r\mathbf{E_{Tr}})/\partial r = 0$. The electric potential in the gap between powered electrode and grounded side-walls $\phi(z=0, R_{\text{powered}} \le r \le R)$ is defined by linear interpolation between $\phi(z=0, r \le R_{\text{powered}}) = V_0 \sin(wt)$ and $\phi(r=R) = 0$.

Note that this model is defined as the full electromagnetic model. In the following, we will compare this model with the so-called electrostatic model, which neglects the effects of the magnetic field and the vortex electric field. This means that in the above equations, only the Poisson equation [Eq. (11)] is solved to obtain the electric field instead of the full set of Maxwell equations, and the magnetic field in Eq. (2) is set to zero.

III. RESULTS AND DISCUSSION

In this part, the influence of the electromagnetic effects on the plasma characteristics is presented for a single frequency CCP operating at various frequencies, voltages, and pressures. The neutral gas temperature is fixed at 300 K. The radius of the upper electrode and lower electrode are $R = 20$ cm and $R_{\text{powered}} = 15$ cm, respectively, and the two electrodes are separated from each other by 3 cm.

A. Frequency effect

The differences between the electrostatic and electromagnetic models at various frequencies will be illustrated by examining the radial distribution of plasma density and electron temperature along the centerline ($z = L/2$) of the reactor, as well as the spatial distribution of the ionization rate. The applied voltage amplitude is 30 V and the pressure is set to 100 mTorr.

The difference between the plasma densities obtained from the electrostatic model and the electromagnetic model, particularly at very high frequencies, is apparent from Fig. 2. In the range of low frequency (i.e., 13.56 MHz), no obvious difference between the plasma density profiles of the two models is detected. Furthermore, in both cases, a slightly higher plasma density appears near the radial reactor edge due to the electrostatic edge effect. This indicates that in this frequency range, the electromagnetic effects are negligible. However, as the frequency increases, the difference between the two density profiles becomes evident, e.g., in the VHF regime, at 60 MHz, shown in Fig. 2(c), the plasma density calculated in the electromagnetic model is nearly twice as high as that in the electrostatic model. Moreover, the electrostatic edge effect becomes less important with increasing frequency,[2] whereas the standing wave effect becomes more dominant, which gives rise to a broad maximum of the plasma density in the center. Especially at the frequency of 100 MHz in Fig. 2(d), the different profiles of plasma density in these two models become obvious. This means that in simulations of discharges sustained by VHF sources, the electromagnetic effects should be taken into account for obtaining realistic results.

In order to understand the different plasma density profiles, the ionization rate distributions obtained from the electromagnetic model at various frequencies are presented in Fig. 3. Note that the ionization rate distribution calculated at 13.56 MHz [Fig. 3(a)] is very similar to the result obtained with the electrostatic model (not shown here), i.e., characterized by a higher ionization rate near the radial edge. This result is obtained in the electrostatic model at all the selected frequencies because only the electrostatic edge effect is taken into account in this case. However, in the electromagnetic model, when the frequency rises, the electrostatic edge effect becomes weaker compared to the standing-wave effect, and thus the ionization occurs mainly in the center at the frequency of 60 MHz, which is responsible for the plasma density being at maximum in the center. When the frequency is 100 MHz, due to the high plasma density obtained in the electromagnetic model, the skin effect becomes more pronounced, which makes the maximum of the ionization rate move again toward the radial edge.

To visualize these electromagnetic effects, the nonuniformity of the axial electric field at the electrode surface ($z = L$) as a function of radial position is illustrated in Fig. 4(a), with the magnitude being normalized by the value at $r=0$. As the frequency increases, the magnitude of the axial electric field rises as well due to the thinner sheath, and the distribution becomes more nonuniform at high frequency (i.e., 60 MHz and 100 MHz), as is obvious from Fig. 4(a). Indeed,

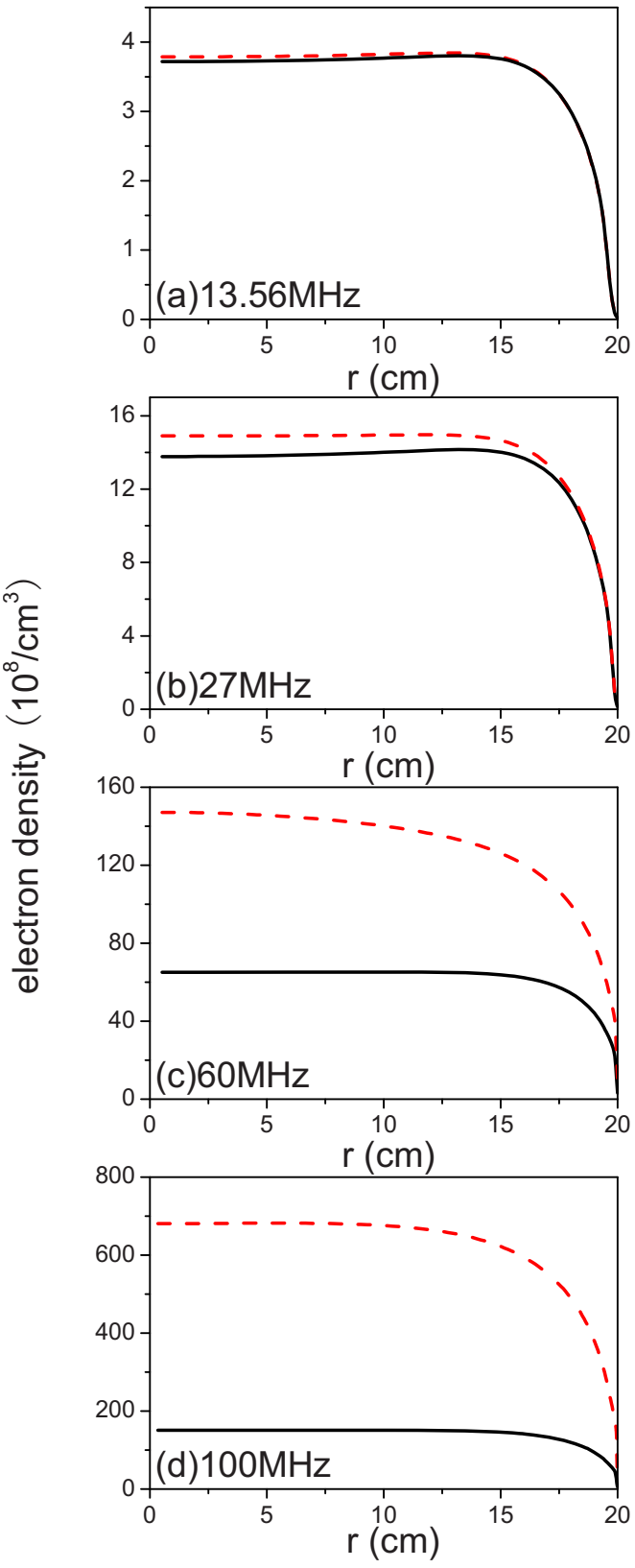

FIG. 2. (Color online) Comparison between the radial distributions of electron density along the reactor centerline ($z=L/2$) in the electrostatic model (solid line) and the electromagnetic model (dashed line) at different frequencies: (a) 13.56 MHz, (b) 27 MHz, (c) 60 MHz, and (d) 100 MHz, for an argon discharge sustained at 100 mTorr and 30 V.

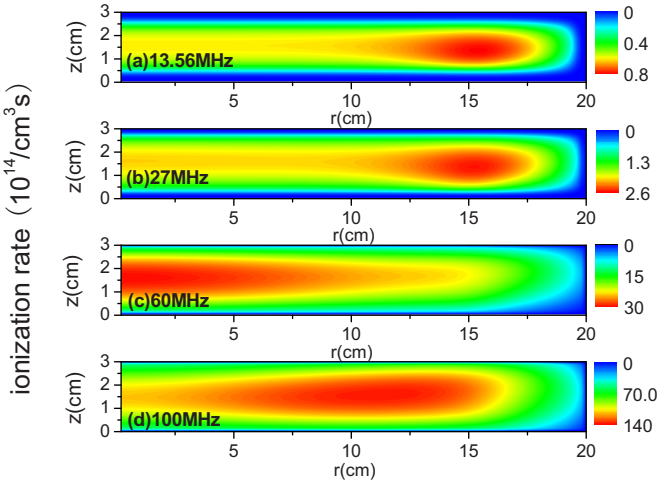

FIG. 3. (Color online) Distributions of ionization rate in the electromagnetic model at different frequencies: (a) 13.56 MHz, (b) 27 MHz, (c) 60 MHz, and (d) 100 MHz, for an argon discharge sustained at 100 mTorr and 30 V.

the electromagnetic wavelength decreases with increasing frequency, and therefore the node of the wave appears near the radial edge, hence diminishing the magnitude of the electric field there, as was also reported in Ref. 33. The dominant standing-wave effect at higher frequency can also be illustrated by examining the integrated power deposition from the axial vortex electric field over the axial direction (i.e., $P_{Tz}=\int_0^L dz\mathbf{E}_{\mathbf{Tz}}\mathbf{j}_{\mathbf{ez}}$). In the range of low frequency, the wavelength is much longer than the reactor radius, so the power deposition caused by the electromagnetic field can be ignored. However, when the frequency is in the VHF regime, the electromagnetic wavelength decreases, and transfers energy to the plasma more efficiently, resulting in a center-peaked power deposition, as is clear from Fig. 4(b). The nonuniform axial electric field, together with the center-peaked power deposition, gives rise to a higher ionization rate in the center at the frequency of 60 MHz. In addition, the magnitude of the radial electric field increases with frequency in the sheath region, as well as the power deposition from the radial vortex electric field, (i.e., $P_{Tr}=\int_0^L dz\mathbf{E}_{\mathbf{Tr}}\mathbf{j}_{\mathbf{er}}$), as shown in Figs. 4(c) and 4(d). Finally, it is obvious from Fig. 4(d) that the power deposition at 100 MHz is more pronounced than at 60 MHz near the radial edge, which indicates that the skin effect is more noticeable at 100 MHz.

To further illustrate the different plasma behavior predicted by the electrostatic model and the electromagnetic model, the spatial profiles of electron temperature are compared at the selected frequency values in Fig. 5. It can be noticed that the distributions of the electron temperature are similar in the two models when the frequency is low because the electromagnetic effects are too weak to have a significant influence on the electron temperature. As the frequency increases to 60 MHz, as shown in Fig. 5(c), the electron temperature achieved in the electromagnetic model is a little higher than in the electrostatic model at the reactor center, but it is lower in the sheath region. Indeed, on one hand, when the electromagnetic effects are considered, the electrons in the bulk plasma are accelerated not only by the electrostatic field, but also by the electromagnetic field, so they

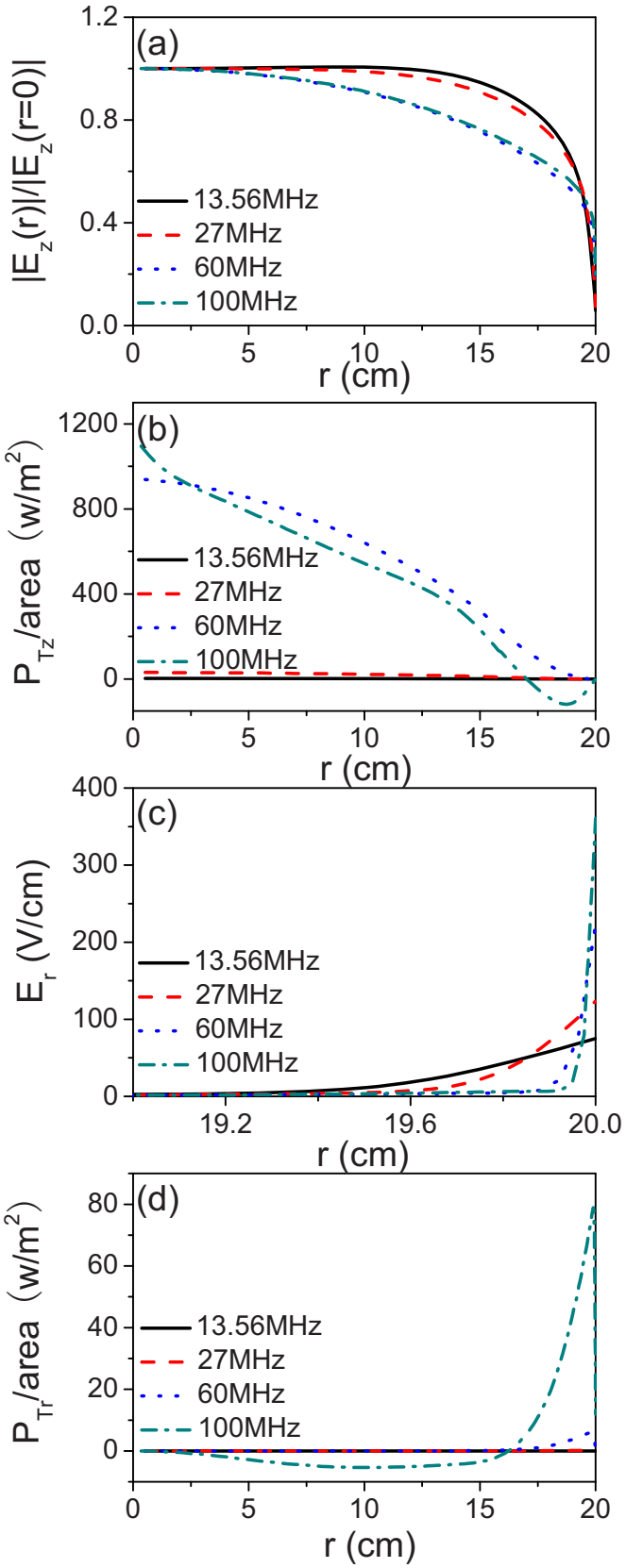

FIG. 4. (Color online) The radial distributions of (a) the axial electric field (normalized by its value at $r=0$) at the electrode surface ($z=L$), (b) the power deposition from the axial vortex electric field, (c) the radial electric field along the reactor centerline ($z=L/2$), and (d) the power deposition from the radial vortex electric field in the electromagnetic model at different frequencies, for an argon discharge sustained at 100 mTorr and 30 V.

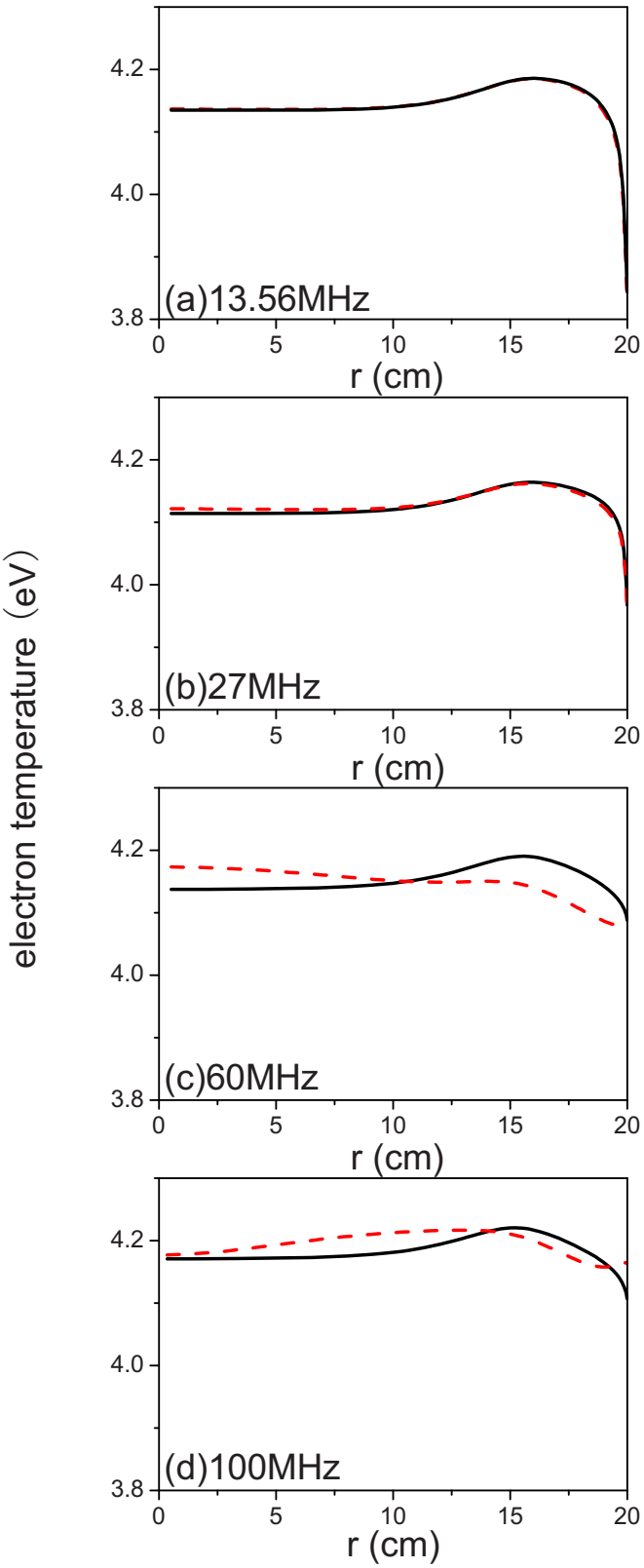

FIG. 5. (Color online) Comparison between the radial distributions of electron temperature along the reactor centerline ($z=L/2$) in the electrostatic model (solid line) and the electromagnetic model (dashed line) at different frequencies: (a) 13.56 MHz, (b) 27 MHz, (c) 60 MHz, and (d) 100 MHz, for an argon discharge sustained at 100 mTorr and 30 V.

may gain more energy than those heated only by the electrostatic field. On the other hand, when the electromagnetic effects are included, the electrons have a shorter distance to be accelerated, accompanied by the limited energy deposition due to the thinner sheath, so the electron temperature is lower in the sheath region.

We also note from Fig. 5 that the electron temperatures achieved in the electromagnetic model at 13.56 and 27 MHz are slightly lower than at 60 and 100 MHz. This may be due to the fact that the electromagnetic power deposition is not remarkable when the frequency is low [see Figs. 4(b) and 4(d)], and the electrons mainly gain energy from the electrostatic power deposition. When the frequency increases from 60 to 100 MHz, the electron temperature increases only slightly. Moreover, the electron temperature rises slightly near the reactor edge in the electromagnetic model at 100 MHz, as shown in Fig. 5(d), due to the significant power deposition caused by the radial electric field, as was illustrated in Fig. 4(d) above.

B. Voltage effect

The plasma characteristics at various voltages calculated by the electrostatic model and the electromagnetic model are plotted to demonstrate the differences between these two models, with the frequency at 100 MHz and the pressure at 100 mTorr.

The radial profiles of plasma density along the reactor centerline ($z=L/2$) are shown in Fig. 6. Compared with the result calculated by the electrostatic model, the profile obtained from the electromagnetic model exhibits a very different shape at all the selected voltages due to the significant electromagnetic effects on the plasma behavior at the frequency of 100 MHz, as mentioned above. In the range of low voltage, e.g., 15 V, the discrepancy between the two models is more noticeable than at higher voltages. Indeed, when the voltage is low, the electrostatic field is relatively weak, and thus the electromagnetic effects are relatively more pronounced. Moreover, strong plasma production occurs at the reactor center in the electromagnetic model at 15 V due to the dominant standing-wave effect. As the voltage increases, shown in Figs. 6(c) and 6(d), the skin effect caused by the high plasma density becomes prominent, hence giving rise to the off-axis peaked plasma density, which is consistent with experiments.[3]

In order to understand the different distributions of plasma density, the ionization rates calculated in the electrostatic and electromagnetic model are illustrated in Figs. 7 and 8, respectively. The ionization rate profiles obtained in the electrostatic model are strikingly different from those in the electromagnetic model, both in shape and especially in absolute values. In the electrostatic model, the edge effect plays a dominant role, and therefore the ionization mainly takes place near the radial edge. On the other hand, in the electromagnetic model, when the voltage is low, the power density from the radial electric field P_r is negligible compared with the power density from the axial electric field P_z, as shown in Fig. 9(a). This indicates that the standing-wave effect is more dominant than the edge effect and the skin

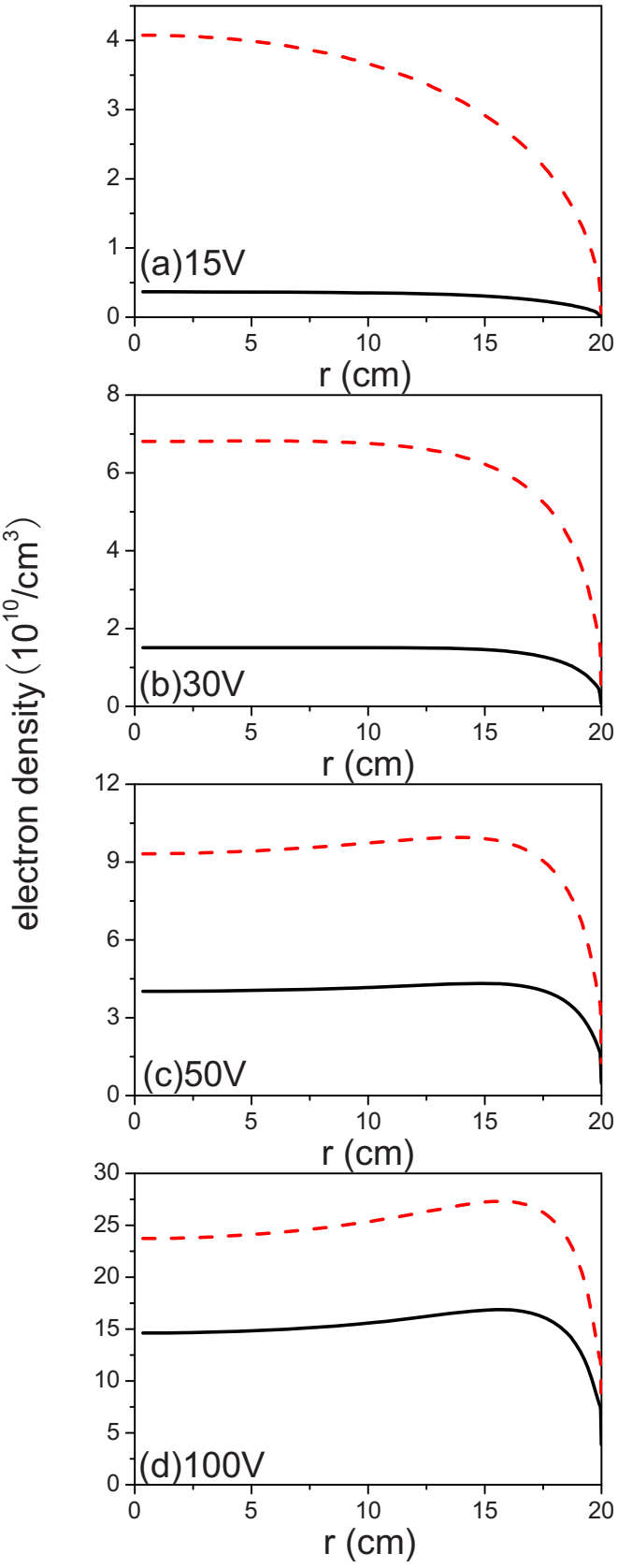

FIG. 6. (Color online) Comparison between the radial distributions of electron density along the reactor centerline ($z=L/2$) in the electrostatic model (solid line) and the electromagnetic model (dashed line) at different voltages: (a) 15 V, (b) 30 V, (c) 50 V, and (d) 100 V, for an argon discharge sustained at 100 MHz and 100 mTorr.

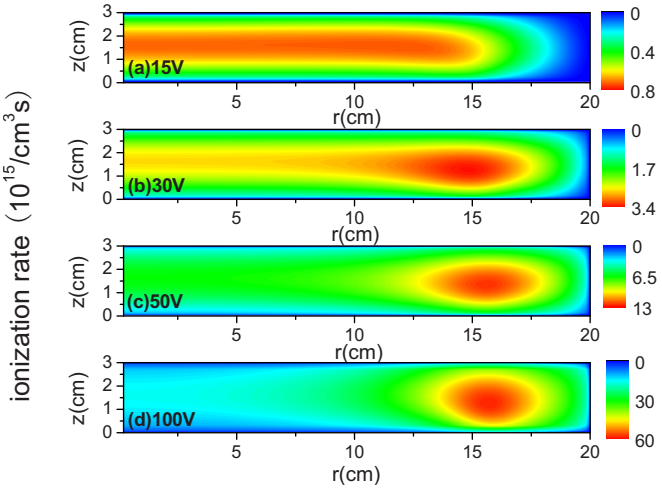

FIG. 7. (Color online) Distributions of ionization rate in the electrostatic model at different voltages: (a) 15 V, (b) 30 V, (c) 50 V, and (d) 100 V, for an argon discharge sustained at 100 MHz and 100 mTorr.

effect, and causes strong plasma production at the reactor center. As the voltage rises, the plasma skin depth is not large compared with the plasma thickness due to the high plasma density, and the so-called radial component of power deposition (P_r) appears to be significant near the radial edge, as seen in Fig. 9(d). This indicates that in this high voltage range, the skin effect rather than the standing-wave effect has a major influence on the discharge behavior. Therefore, the ionization rate shifts from center-peaked to off-axis peaked with increasing voltage (cf. Fig. 8), which explains the plasma density evolution illustrated in Fig. 6.

The spatial distributions of electron temperature, calculated in the electrostatic and electromagnetic model, are compared at the selected voltage values in Fig. 10. When the voltage is low, the electron temperature in the electromagnetic model is slightly higher than in the electrostatic model at the center region, but it is lower near the radial edge, and then shows a slightly higher value again close to the wall. As the voltage increases, the difference between the electron

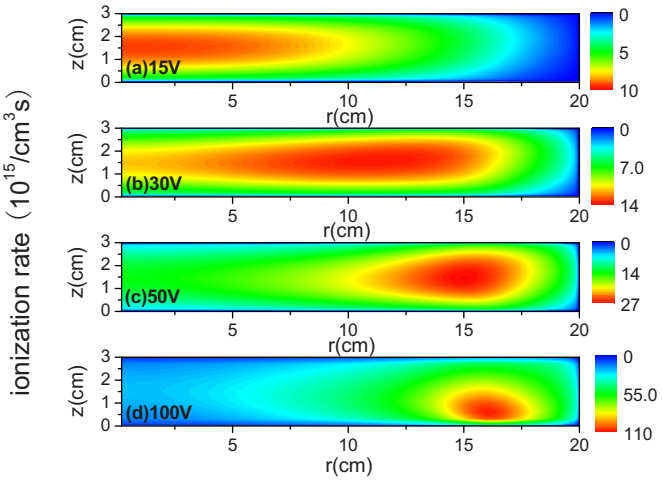

FIG. 8. (Color online) Distributions of ionization rate in the electromagnetic model at different voltages: (a) 15 V, (b) 30 V, (c) 50 V, and (d) 100 V, for an argon discharge sustained at 100 MHz and 100 mTorr.

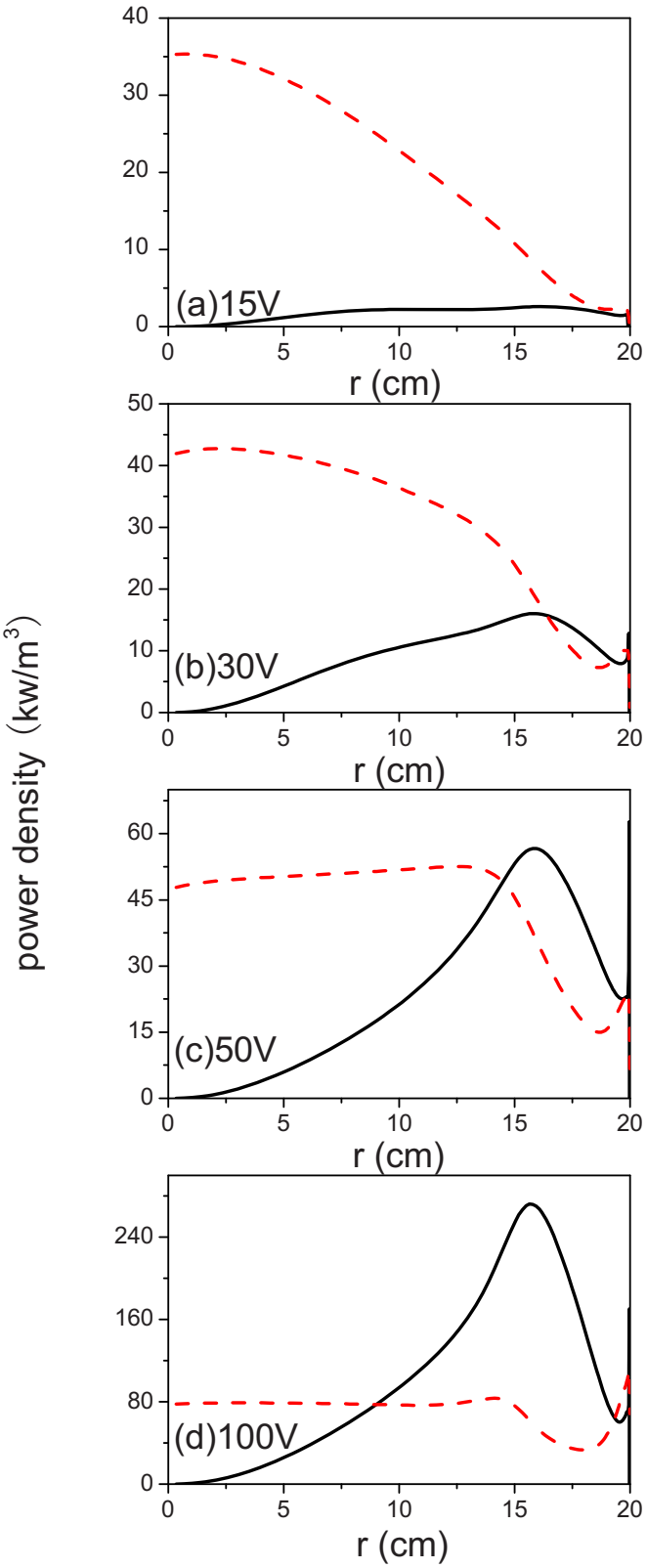

FIG. 9. (Color online) Comparison between the radial distributions of power density from the radial electric field (solid line) and the axial electric field (dashed line) along the reactor centerline ($z=L/2$) in the electromagnetic model at different voltages: (a) 15 V, (b) 30 V, (c) 50 V, and (d) 100 V, for an argon discharge sustained at 100 MHz and 100 mTorr.

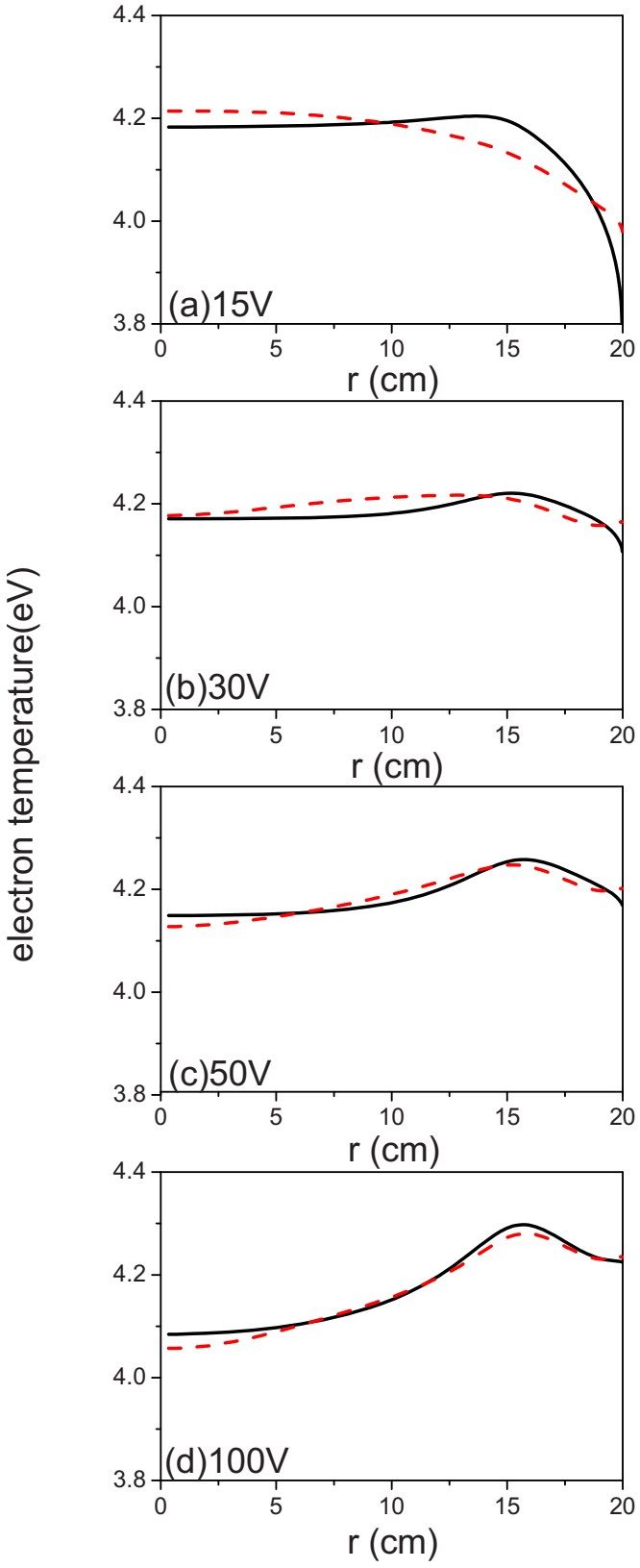

FIG. 10. (Color online) Comparison between the radial distributions of electron temperature along the reactor centerline ($z=L/2$) in the electrostatic model (solid line) and the electromagnetic model (dashed line) at different voltages: (a) 15 V, (b) 30 V, (c) 50 V, and (d) 100 V, for an argon discharge sustained at 100 MHz and 100 mTorr.

temperature in the two models becomes less apparent. Moreover, the electron temperature in the electromagnetic model decreases a little at the center, and increases slightly near the radial edge, shifting from center high to edge high with increasing voltage. Indeed, on one hand, the energy gain is limited by the more frequent ionization collisions; on the other hand, the electrons will gain more energy from the significant radial component of power deposition in the sheath [see Fig. 9(d)].

C. Pressure effect

Finally, the electromagnetic effects on the plasma characteristics are examined at different pressures, with the frequency at 100 MHz and the voltage set to 30 V. The evolution of plasma density, as a function of pressure, is shown in Fig. 11. Since the electromagnetic effects are remarkable in the high frequency range, the difference between the plasma density in the two models is obvious, at all pressures investigated. When the pressure is low, i.e., 50 mTorr, the plasma density in the electromagnetic model is slightly higher near the radial edge of the reactor, see Fig. 11(a). This is because the plasma density profile is determined by both the electromagnetic effects and the edge effect. Although the standing wave effect caused by the VHF power may produce the plasma mainly at the reactor center, the electrostatic power deposition is dominant under this condition, and accordingly the plasma density is slightly higher near the electrode edge. However, the plasma spatial profile evolves to a broad maximum in the center at the higher pressure of 1 Torr, as is clear in Fig. 11(d). The reason is that the edge effect is limited when the pressure is high, so the electromagnetic effects play a more important role.

The different plasma density distributions along the centerline can be explained by examining the evolution of ionization rate obtained in the electrostatic and electromagnetic model at various pressures in Figs. 12 and 13, respectively. In the electrostatic model, the ionization mainly occurs near the radial edge at low pressure (see Fig. 12). When the pressure increases, the ionization rate distribution becomes more uniform, which indicates that the edge effect is limited at high pressure (see below). Indeed, the radial electrostatic field in the sheath region becomes weaker, as seen in Fig. 14(a). When the electromagnetic effects are taken into account (see Fig. 13), the plasma production also mainly takes place near the reactor edge at low pressure, hence explaining the plasma density profile of Fig. 11(a). As the pressure increases, the axial electric field at the electrode surface ($z=L$) becomes nonuniform, with the magnitude diminishing near the radial edge [see Fig. 14(c)]. Moreover, the so-called axial component of power density exhibits a maximum at the reactor center, as seen in Fig. 14(d). This means that the edge effect is limited, and meanwhile the standing-wave effect becomes dominant with increasing pressure. Thus the maximum of the ionization rate shifts to the reactor center, as is clear from Fig. 13(d).

The different evolutions of electron temperature with pressure in the two models are depicted in Fig. 15. At the low pressure of 50 mTorr, the electron temperature obtained

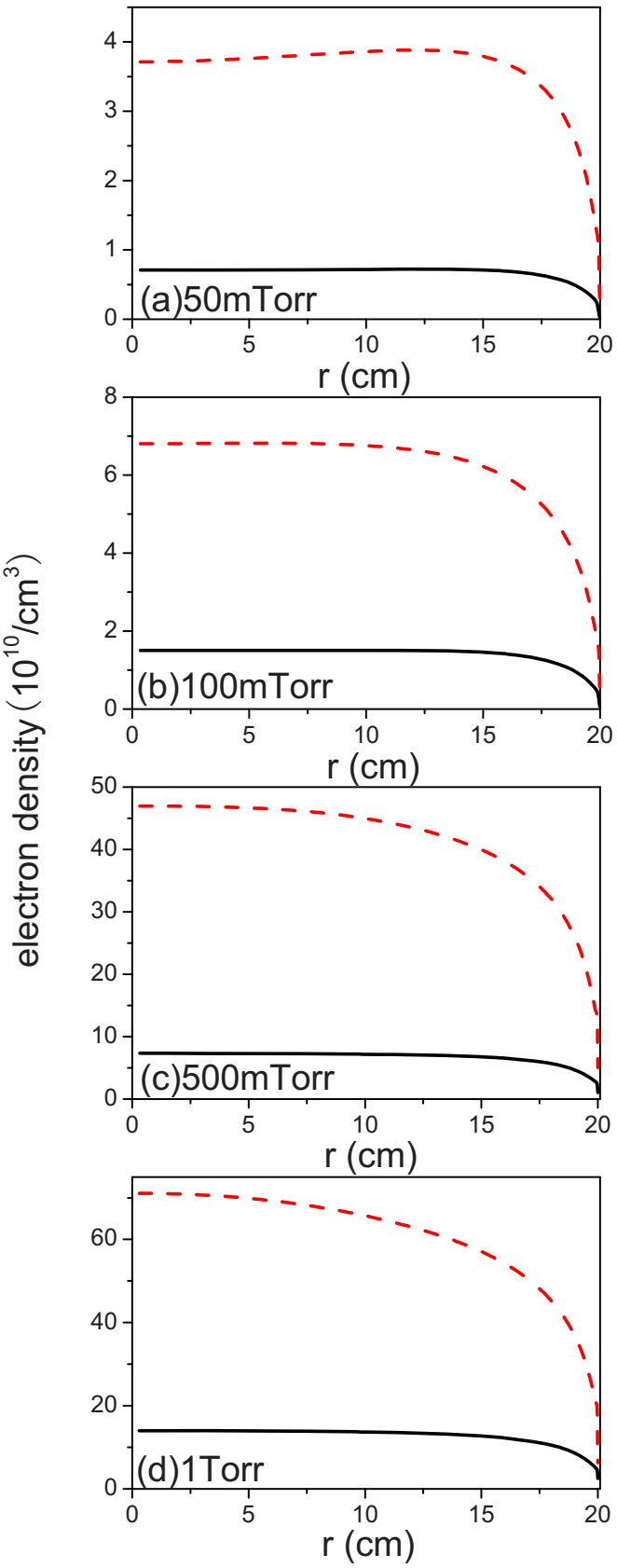

FIG. 11. (Color online) Comparison between the radial distributions of electron density along the reactor centerline ($z=L/2$) in the electrostatic model (solid line) and the electromagnetic model (dashed line) at different pressures: (a) 50 mTorr, (b) 100 mTorr, (c) 500 mTorr, and (d) 1 Torr, for an argon discharge sustained at 100 MHz and 30 V.

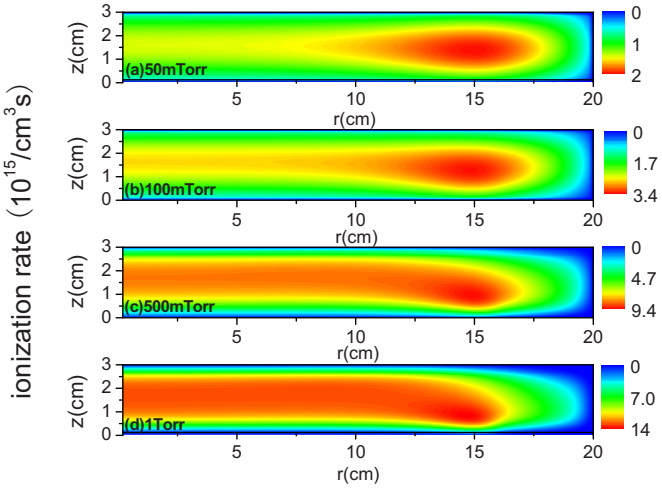

FIG. 12. (Color online) Distributions of ionization rate in the electrostatic model at different pressures: (a) 50 mTorr, (b) 100 mTorr, (c) 500 mTorr, and (d) 1 Torr, for an argon discharge sustained at 100 MHz and 30 V.

in the electromagnetic model is slightly lower than that in the electrostatic model, except at around 10 cm from the discharge axis. As the pressure increases, the electron temperature is a little higher than in the electrostatic model in the center region, but it is lower near the radial edge, as we have also analyzed in Fig. 5(c). In addition, the electron temperature shifts from edge high to center high because the standing-wave effect rather than the edge effect has a dominant influence on the discharge in the high pressure case.

IV. CONCLUSIONS

In this paper, a two-dimensional self-consistent fluid model, which includes the full set of Maxwell equations, is developed to investigate the influence of electromagnetic effects on the characteristics of a capacitively coupled Ar plasma. The differences between the electrostatic model and the electromagnetic model have been illustrated by examin-

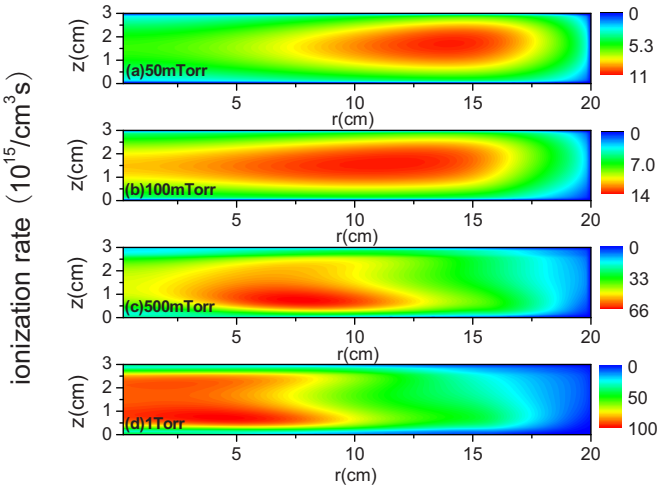

FIG. 13. (Color online) Distributions of ionization rate in the electromagnetic model at different pressures: (a) 50 mTorr, (b) 100 mTorr, (c) 500 mTorr, and (d) 1 Torr, for an argon discharge sustained at 100 MHz and 30 V.

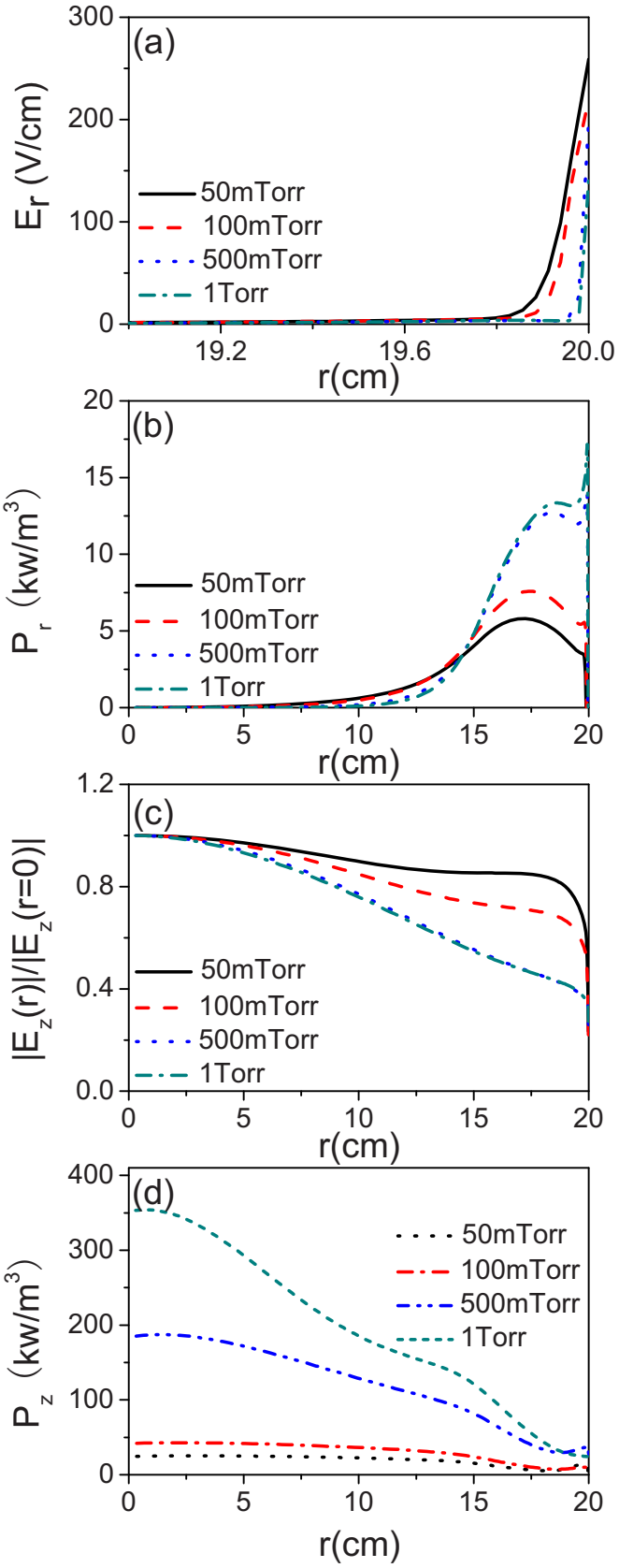

FIG. 14. (Color online) The radial distributions of (a) the radial electric field along the reactor centerline ($z=L/2$) in the electrostatic model, (b) the power density from the radial electric field along the reactor centerline ($z=L/2$) in the electrostatic model, (c) the axial electric field (normalized by its value at $r=0$) at the electrode surface ($z=L$) in the electromagnetic model, and (d) the power density from the axial electric field along the reactor centerline ($z=L/2$) in the electromagnetic model at different pressures, for an argon discharge sustained at 100 MHz and 30 V.

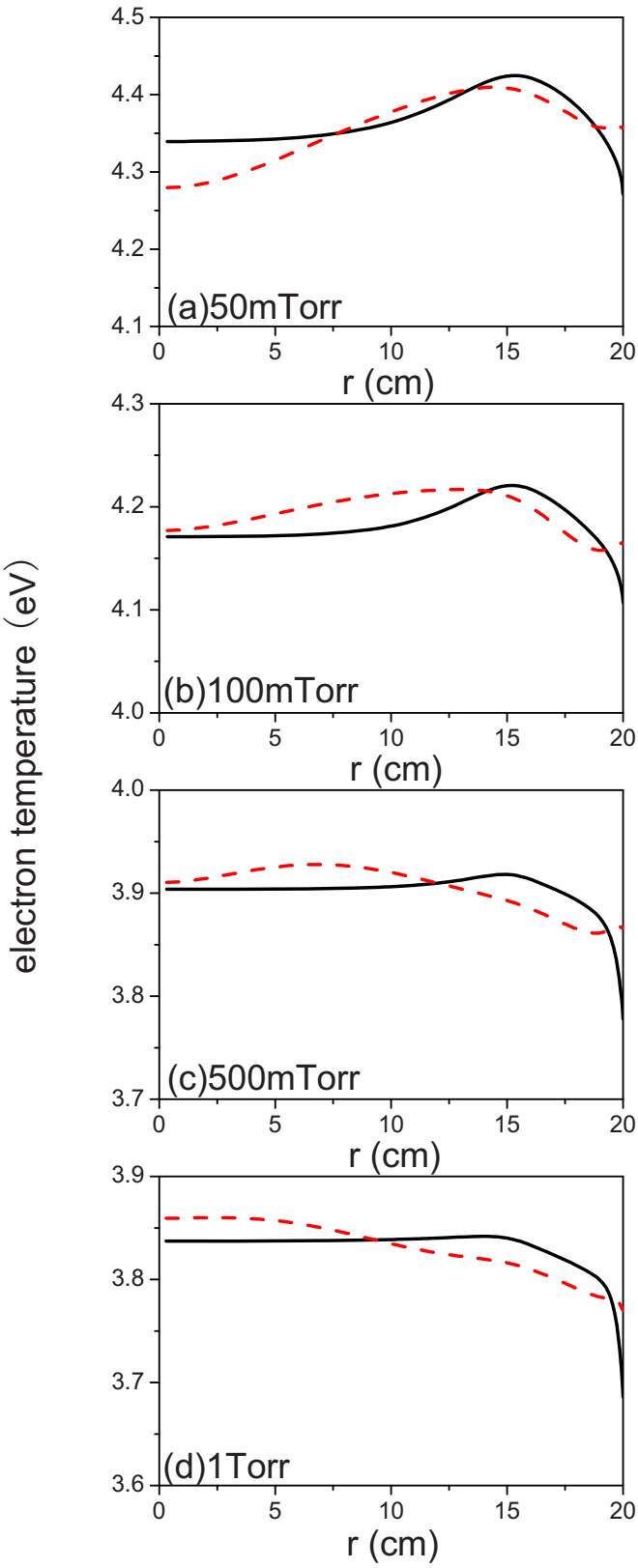

FIG. 15. (Color online) Comparison between the radial distributions of electron temperature along the reactor centerline ($z=L/2$) in the electrostatic model (solid line) and the electromagnetic model (dashed line) at different pressures: (a) 50 mTorr, (b) 100 mTorr, (c) 500 mTorr, and (d) 1 Torr, for an argon discharge sustained at 100 MHz and 30 V.

ing the distribution of plasma density, ionization rate, and electron temperature for different values of frequency, voltage, and pressure.

As is illustrated by this comparison, it is essential to simulate the VHF discharge by taking into account the electromagnetic effects, due to the significant differences between the plasma characteristics obtained by the electrostatic and electromagnetic models, especially at VHF. The plasma density profile in the electrostatic model is similar to that in the electromagnetic model in the range of lower frequency (i.e., 13.56 MHz), but as the frequency increases, the difference becomes obvious. At the frequency of 100 MHz, the plasma density in the electromagnetic model is nearly four times as high as that in the electrostatic model, and it exhibits a broad maximum in the center, since the electromagnetic effects rather than the edge effect have a major impact on the discharge under the high frequency condition. A similar behavior is seen for the ionization rate and electron temperature. The electron temperature seems less dependent on frequency; a significant difference is only observed when the frequency rises from 27 to 60 MHz.

We have also investigated the electromagnetic effects on the plasma conditions at different voltages and pressures, when the frequency is kept fixed at 100 MHz. In the high voltage case, the difference between these two models is less pronounced, but as the voltage decreases, the difference becomes obvious. This is because the electrostatic field is weaker at lower voltage, thus the electromagnetic effects have a relatively larger influence on the plasma behavior. In the electromagnetic model, the radial profile of plasma density varies from center-peaked to off-axis peaked with increasing voltage because the skin effect rather than the standing-wave effect is dominant at high voltage. In addition, when the pressure is low, the highest plasma density appears near the radial edge in both the electrostatic and electromagnetic models, but still it exhibits very different shapes, since the electromagnetic effects are significant in the VHF case. As the pressure increases, the profile of plasma density along the centerline obtained in the electrostatic model becomes uniform due to the limited edge effect. On the other hand, when the electromagnetic effects are taken into account, the plasma production is more pronounced at the center. In conclusion, the differences between the calculation results obtained with the electrostatic and electromagnetic models indicate that the electromagnetic effects are very important for the discharge, and cannot be ignored in simulations, in order to obtain realistic results, especially when the plasma is sustained by a VHF source.

ACKNOWLEDGMENTS

This work was supported by the National Natural Science Foundation of China (Grant Nos. 10635010 and 10805008), the Specialized Research Fund for the Doctoral Program of Higher Education (Grant No. 20090041110026), and the joint research project in the framework of the agreement between MOST and FWO.

[1] J. W. Coburn, IEEE Trans. Plasma Sci. **19**, 1048 (1991).
[2] T. Kitajima, Y. Takeo, N. Nakano, and T. Makabe, J. Appl. Phys. **84**, 5928 (1998).
[3] A. Perret, P. Chabert, J.-P. Booth, J. Jolly, J. Guillon, and Ph. Auvray, Appl. Phys. Lett. **83**, 243 (2003).
[4] A. A. Howling, J.-L. Dorier, Ch. Hollenstein, U. Kroll, and F. Finger, J. Vac. Sci. Technol. A **10**, 1080 (1992).
[5] L. Sansonnens, A. Pletzer, D. Magni, A. A. Howling, Ch. Hollenstein, and J. P. M. Schmitt, Plasma Sources Sci. Technol. **6**, 170 (1997).
[6] M. A. Lieberman, J. P. Booth, P. Chabert, J. M. Rax, and M. M. Turner, Plasma Sources Sci. Technol. **11**, 283 (2002).
[7] L. Sansonnens and J. Schmitt, Appl. Phys. Lett. **82**, 182 (2003).
[8] L. Sansonnens, J. Appl. Phys. **97**, 063304 (2005).
[9] P. Chabert, J.-L. Raimbault, P. Levif, J.-M. Rax, and M. A. Lieberman, Phys. Rev. Lett. **95**, 205001 (2005).
[10] P. Chabert, J.-L. Raimbault, P. Levif, J.-M. Rax, and M. A. Lieberman, Plasma Sources Sci. Technol. **15**, S130 (2006).
[11] I. Lee, D. B. Graves, and M. A. Lieberman, Plasma Sources Sci. Technol. **17**, 015018 (2008).
[12] S. Rauf, K. Bera, and K. Collins, Plasma Sources Sci. Technol. **17**, 035003 (2008).
[13] K. Bera, S. Rauf, K. Ramaswamy, and K. Collins, J. Vac. Sci. Technol. A **27**, 706 (2009).
[14] Z. Chen, S. Rauf, and K. Collins, J. Appl. Phys. **108**, 073301 (2010).
[15] V. Georgieva and A. Bogaerts, J. Appl. Phys. **98**, 023308 (2005).
[16] V. Georgieva and A. Bogaerts, Plasma Sources Sci. Technol. **15**, 368 (2006).
[17] K. Bera, S. Rauf, K. Ramaswamy, and K. Collins, J. Appl. Phys. **106**, 033301 (2009).
[18] X. Xu, S. X. Zhao, Y. R. Zhang, and Y. N. Wang, J. Appl. Phys. **108**, 043308 (2010).
[19] Y. Yang and M. J. Kushner, J. Phys. D: Appl. Phys. **43**, 152001 (2010).
[20] Y. Yang and M. J. Kushner, Plasma Sources Sci. Technol. **19**, 055011 (2010).
[21] Y. Yang and M. J. Kushner, Plasma Sources Sci. Technol. **19**, 055012 (2010).
[22] K. Satake, H. Yamakoshi, and M. Noda, Plasma Sources Sci. Technol. **13**, 436 (2004).
[23] H. Schmidt, L. Sansonnens, A. A. Howling, Ch. Hollenstein, M. Elyaakoubi, and J. P. M. Schmitt, J. Appl. Phys. **95**, 4559 (2004).
[24] L. Sansonnens, H. Schmidt, A. A. Howling, Ch. Hollenstein, Ch. Ellert, and A. Buechel, J. Vac. Sci. Technol. A **24**, 1425 (2006).
[25] P. A. Miller, E. V. Barnat, G. A. Hebner, A. M. Paterson, and J. P. Holland, Plasma Sources Sci. Technol. **15**, 889 (2006).
[26] G. A. Hebner, E. V. Barnat, P. A. Miller, A. M. Paterson, and J. P. Holland, Plasma Sources Sci. Technol. **15**, 879 (2006).
[27] S. K. Ahn and H. Y. Chang, Appl. Phys. Lett. **93**, 031506 (2008).
[28] D. Sung, S. Jeong, Y. Park, V. N. Volynets, A. G. Ushakov, and G.-H. Kim, J. Vac. Sci. Technol. A **27**, 13 (2009).
[29] D. Sung, J. Woo, K. Lim, K. Kim, V. Volynets, and G.-H. Kim, J. Appl. Phys. **106**, 023303 (2009).
[30] V. Volynets, H. Shin, D. Kang, and D. Sung, J. Phys. D: Appl. Phys. **43**, 085203 (2010).
[31] E. Gogolides and H. H. Sawin, J. Appl. Phys. **72**, 3971 (1992).
[32] J. D. Bukowski, D. B. Graves, and P. Vitello, J. Appl. Phys. **80**, 2614 (1996).
[33] L. Sansonnens, A. A. Howling, and Ch. Hollenstein, Plasma Sources Sci. Technol. **15**, 302 (2006).